DOI: 10.21062/mft.2023.005 http://www.journalmt.com

Topology Optimization of Static Turbomachinery Components

Francesco Buonamici (0000-0001-5186-9724), Enrico Meli (0000-0002-0513-9242), Nicola Secciani (0000-0003-4207-2451), Alessandro Ridolfi (0000-0001-8493-7594), Andrea Rindi (0000-0001-7779-752X), Rocco Furferi (0000-0001-6771-5981)
Department of Industrial Engineering of Florence. Via di S. Marta 3, 50139 Florence, Italy. E-mail: francesco.buonamici@unifi.it

Additive Manufacturing has enabled the design of complex components in several technical fields. Considering turbomachinery components, additive manufacturing has unlocked the achievement of significant performances for dynamic rotoring components. The application of topology optimization methods is one of the main factors accelerating the technological development of this sector. This paper presents a procedure for the optimization of static turbomachinery components. The framework proposed compares the results obtained by introducing a lattice structure and a solid optimized shape. The procedure is presented with reference to a specific case study. To validate the proposed framework, the complete re-design of a thrust collar of a major Italian-based Oil&Gas company is carried out, demonstrating that the re-thinking of the component in terms of Topology Optimization is a straightforward approach to increase the overall performance of the produced part.

Keywords: Topology optimization, turbomachinery, thrust washer, dynamic optimization

1 Introduction

Modern Additive Manufacturing (AM) technologies are classified among the driving factors of the fourth industrial revolution. Their implementation in the turbomachinery world has unlocked a more sustainable manufacturing approach [1] and it has allowed the production of components characterized by high performances/weight ratios thanks to the manufacturability of lattice structures[2], hollowed shapes. Such advantages have brought to the development of innovative design approaches and tools. Among these, Topology Optimization (TO) has carved out the most relevant space and has established itself as the to-go methodology when the design of high-performance lightweight components is requested.

While its potential is proven, the application of a full TO/AM workflow to real-cases is still only partially documented in the scientific literature, probably due to commercial interests and the costs associated with the production of full-scale turbomachinery components. Accordingly, there is significative interest for the discussion of methodological approaches and techniques for the design of turbomachinery components. Nonetheless, TO turbomachinery applications are still documented in the scientific literature, although limited occurrences can be found (e.g. [3]–[5]). For the interested reader, [6] offers a full review on the topic.

The application of the TO methodology in this field unlocks positive side-effects beside the pure mass reduction: the trial and error phase necessary to identify the optimal design is considerably reduced, since the morphology obtained for a given component is directly related to the load it musts support and to the imposed goal. Moreover, thanks to the mass reduction, material costs are lowered; AM technologies also allows for a full automated production phase which, although it requires a long time, can be performed practically

The procedure proposed in the present study integrates the design phase with the production via additive manufacturing processes in order to assure the achievement of a high-quality result. The procedure is innovative in several respects; among them, the inclusion of contact forces caused by forced coupling on the shaft of the component of interest. This aspect requires the definition of contact surfaces within the optimization. Two different optimizations were carried out in order to achieve this goal: a static linear optimization and a non-linear one; this latter is capable of computing and considering contact forces throughout the iterations and therefore, should offer more accurate results. The test case used in this study have been produced by the Turbomachinery Engineering Department of Baker Hughes, General Electric Oil&Gas; specifically, by Nuovo Pignone.

2 The case study

The case study considered in this article is the structural optimization of a thrust washer supplied by the Turbomachinery Engineering Department of

ISSN 1213–2489
e-ISSN 2787–9402

Baker Hughes, General Electric Oil&Gas, Nuovo Pignone. The component is positioned as showed in Fig.1 within a centrifugal compressor. In the following, the component will be presented both from a geometrical perspective and functional requirements.

The disc is fabricated in IN718 and forced on its housing with an interference of 1.4 ‰ with respect to the radius of the shaft, and the contact surfaces are lapped and chamfered to avoid losses due to friction. The dimensions of the original component are shown in Fig. 2.

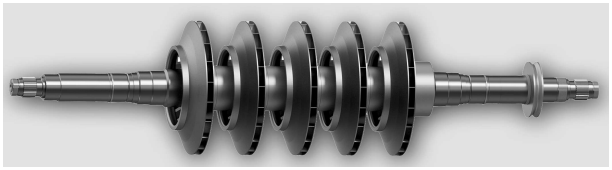

Fig. 1 *Position of the thrust collar component (on the right in gold) in the centrifugal compressor rotor assembly*

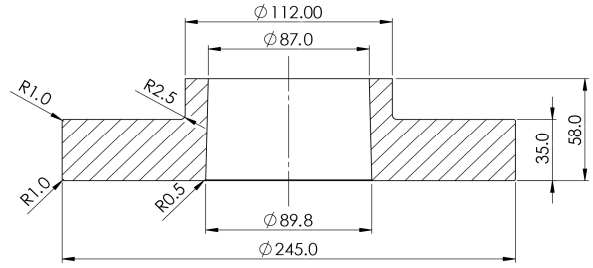

Fig. 2 *Geometry of the original thrust collar prior to the optimization. Diametral section with dimension expressed in mm*

The component is stressed by two fixed loads: a centrifugal load and a pressure load that is distributed on the contact internal area. Moreover, there is an axial load, generated by the pressure differentials created by the machine, whose direction is variable depending on the working conditions of the machine.

Angular speed is 16100 rpm (1686 rad/s). The modulus of the axial load is 90000 N. Conversely to the approach followed in [4], no dynamic effects have been considered in this study due to the high stiffness of the original part. On the other hand, dynamic effects cannot be completely overlook on the future optimized part; the optimization aims at minimizing the mass. Topology-optimized parts are typically characterized by slender geometries and sections characterized by low thicknesses; accordingly, it will be necessary to verify that this operation does not cause the insurgence of vibration modes with a natural frequency that may be included in the operating range of the machine.

3 Methodology

Two different optimizations were performed: a linear one and a non-linear one. This second optimization is performed to simulate also the force coupling between the washer and the shaft. Accordingly, the linear optimization only considers the main component, while the non-linear analysis requires the additional definition of the shaft model.

The original CAD model of the part was modelled using the parametric 3D CAD modeler Solidworks by Dassault Systèmes®. All the FE modeling and analysis was performed within Altair Hypermesh.

The first operation performed on the model is the definition of design and non-design regions; this allows the distinction between the volume which will be modified by the optimization algorithm and the parts that will be maintained untouched. The non-design region was defined as an offset of the part's external surface of XX mm; moreover, an additional external disk positioned in the middle of the bigger cylinder was included in the design space. Such space was preserved to account for future balancing holes that will be made in the refinement stage of production. A Tetrahedral mesh with dimension of 3 mm was selected, by performing preliminary tests, as the ideal configuration to obtain a valid result. The resulting mesh is visible in the diameter sectional view reported in Fig. 3. Quality controls were applied to obtain a validation of the mesh. The material properties assigned to the material are summarized in Table 1.

Tab. 1 *Design material properties*

Elastic Modulus	220000 MPa
Poisson Coefficient (ν)	0.3
Density (ρ)	7850 kg/m^3

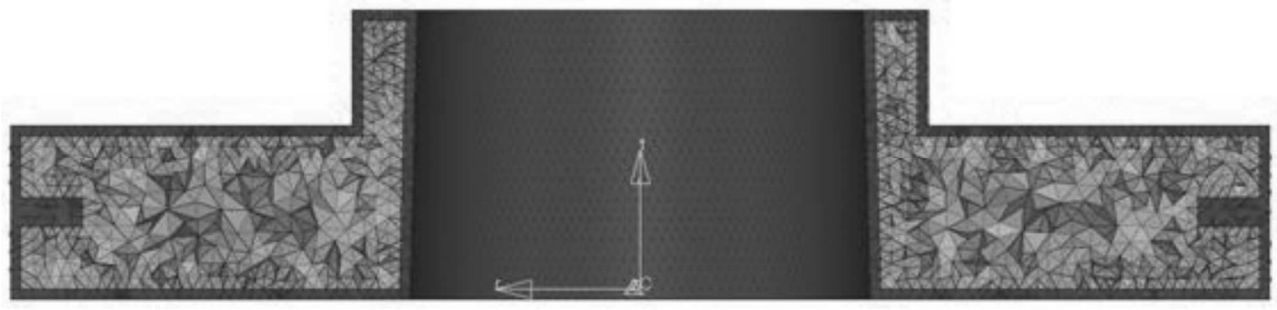

Fig. 3 *Diametral section of the meshed component; tetrahedral elements were used to model the solid*

indexed on http://www.webofscience.com and http://www.scopus.com

Single Point Constraints (SPCs) was used to limit the Degrees of Freedom (DoFs) of the nodes of interest. Two different constraint scenarios are in particular used, one for the linear static optimization and the second one for the non-linear one, which requires the introduction of a shaft portion. The shaft was modelled using hexahedral elements to obtain a uniform distribution of the elements and reduce element penetration issues. The constraint scheme used for the linear static optimization is depicted in Fig. 4a, while the non-linear constraint setup is depicted in Fig. 4b; in this case, axial constraints are imposed on the faces of the shaft and not directly on the thrust collar as in the first case. It should be noted that in the optimization case that takes into account the force coupling, the nonlinearity of the analysis is given only by the presence of the contacts, and therefore affects the first loadstep where a temperature difference is applied on the model to promote the expansion of the parts. Once the forcing process is complete, the subsequent loading conditions begin by starting with the result of stresses and displacements from the nonlinear analysis.

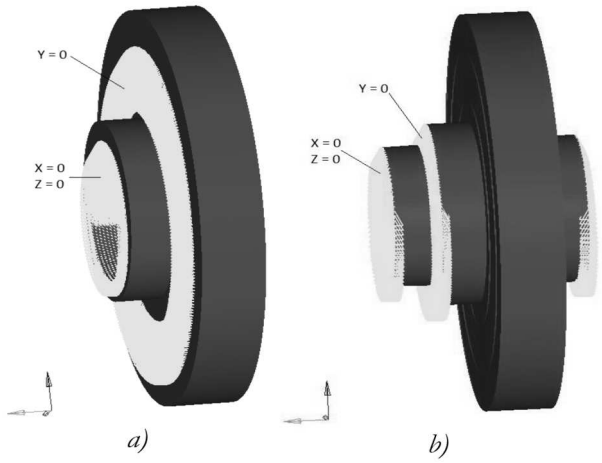

Fig. 4 *Constraint setup for the a) linear optimization and b) for the non-linear optimization; constrained nodes are depicted in yellow; labels clarify which directions are limited for every group of nodes*

3.1 Load cases

The axial compression load of 90000N is distributed on the non-constrained face of the collar, resulting on a pressure load of 6.80MPa. The centrifugal load is applied by means of the definition of a cylindrical set of coordinates and setting a rotation speed of 16100 rpm. The shaft/ring coupling with interference is simulated introducing a thermal expansion effect.

Table 2 reports a summary of the load cases considered in the analyses; each load case is indicated by a numerical index and indicating the direction of application according to the reference frame depicted in Fig. 4.

Tab. 2 *Load Cases*

Index	Load Cases
1	Axial Load (-Y)
2	Axial Load (+Y)
3	Centrifugal Load (-Y)
4	Combined Load (1+3)
5	Combined Load (2+3)

3.2 Static linear optimization

A first round of optimization was carried out by imposing as optimization goal the minimization of the compliance under a single load case scenario and by imposing the additional constraint of limiting the minimum amount of material to be removed while performing the optimization. A 30% of the original mass value was set as constraint. Load cases #1 #2 and #3 were tested independently; the response of each optimized model to the other loads configuration was then tested with additional FE analyses. Related results are reported in Table 3. Figures 5 to 7 show the results obtained in terms of mass distributions and shapes generated by the optimization. Obviously, such geometries are only first-attempt results required for the description of the problem, as no one of these models is optimized to whitstandt load cases different from the single one used to drive the optimization.

Tab. 3 *Results of Static Linear Optimization with load cases #1, #2 and #3 (Stresses and displacements); dark edged cells present the results obtained using the load cases driving the optimization*

Index	Load Case used to drive optimization	Response	Verified under		
			Axial Load #1	Axial Load (#2)	Centrifugal Load (#3)
A	1	Stress (MPa)	81	263	248
		Displacement mag. (mm)	0.0331	0.1795	0.1070
B	2	Stress (MPa)	186	83	247
		Displacement mag. (mm)	0.1539	0.0328	0.1069
C	3	Stress (MPa)	264	265	122
		Displacement mag. (mm)	0.1931	0.2001	0.0030

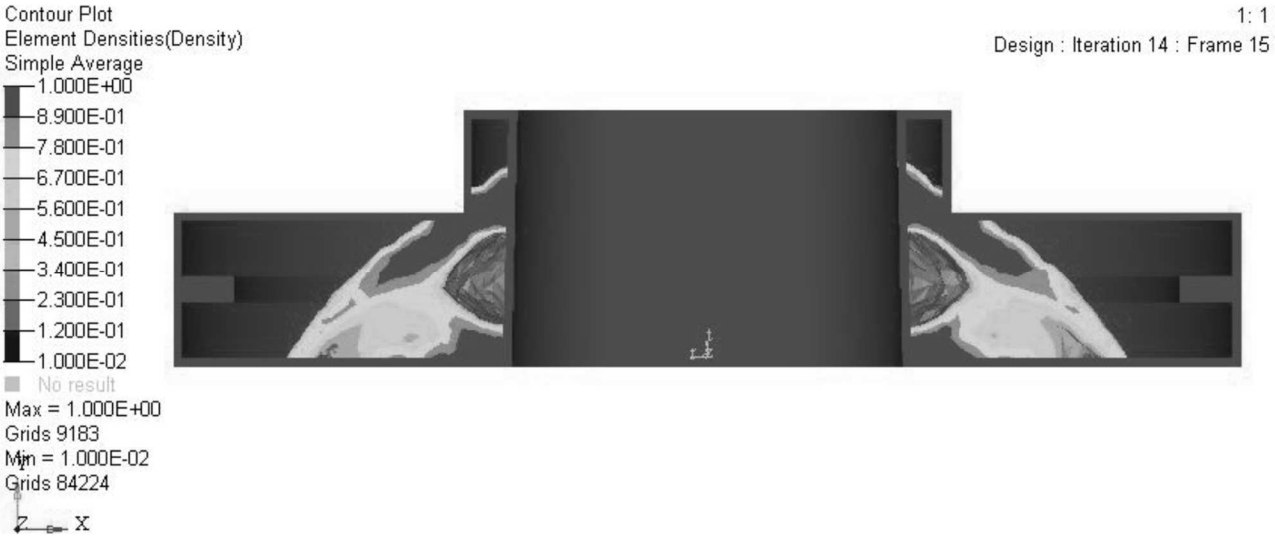

Fig. 5 *Mass distribution obtained for Load case 1*

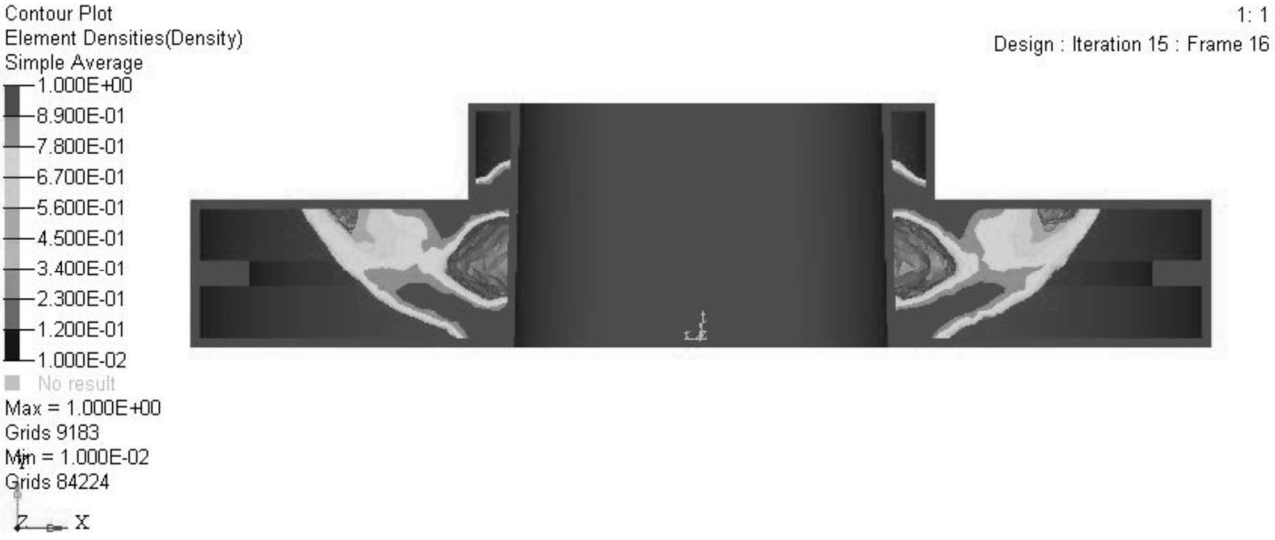

Fig. 6 *Mass distribution obtained for Load case 2*

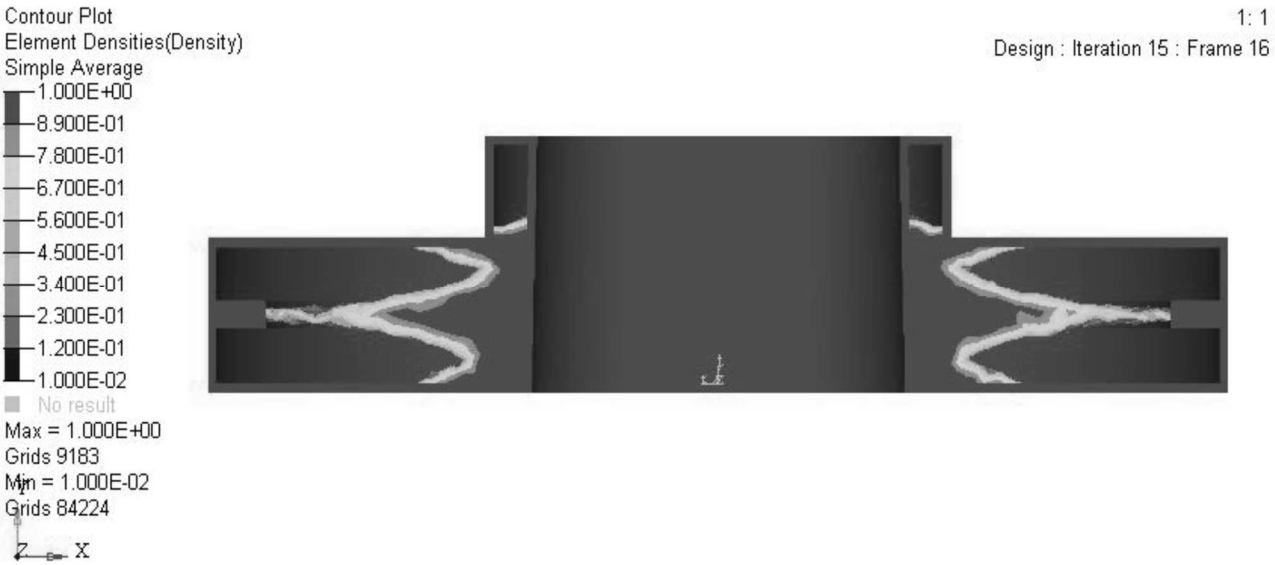

Fig. 7 *Mass distribution obtained for Load case 3*

After this first step, combined loads were used to consider a more realistic scenario, where the three components are introduced. In order to achieve this result, a weighted compliance was considered to drive the analysis. All loads were weighted equally with a unitary weight value. A 30% volume fraction of the original design space was used to constrain the analysis.

The first weighted optimization produced the mass distribution depicted in Fig. 8, which is roughly a sum of the previous three distributions. Stress and displacements results are reported in Table 4. The results show a behaviour of the component that is optimized for all the load cases, showing the efficacy of the approach.

Fig. 8 *Mass distribution obtained for the weighted compliance - D*

Tab. 4 *Stress and displacement values for weighted compliance simulations*

INDEX	Optimization driving factor	Constraint	Response	Verified under		
				Axial Load #1	Axial Load (#2)	Centrifugal Load (#3)
D	Weighted Compliance (1,1,1)	30% volume fraction	Stress (MPa)	69	68	117
			Displacement mag. (mm)	0.0447	0.0445	0.0349
E	Weighted Compliance (1,1,1) + constraint minimum size	30% volume fraction, minimum member size = 3*mesh size	Stress (MPa)	108	111	178
			Displacement mag. (mm)	0.0699	0.0690	0.0433

From the analysis of the geometry produced by the optimizer, it was identified the requirement for the introduction of a control parameter limiting the generation of discontinuous structures with limited connections with the other parts of the component. Accordingly, a control parameter defining the minimum dimension of the element generated within the design zone was set equal at three times the mesh size. Related results are reported in row "E" of table 4. This solution is less effective compared with D, but generates a component with a higher manufacturability and less prone to problems such as distortions, low fatigue life, fabricability. Additional experiments performed changing the value of such control parameter showed no significant effects.

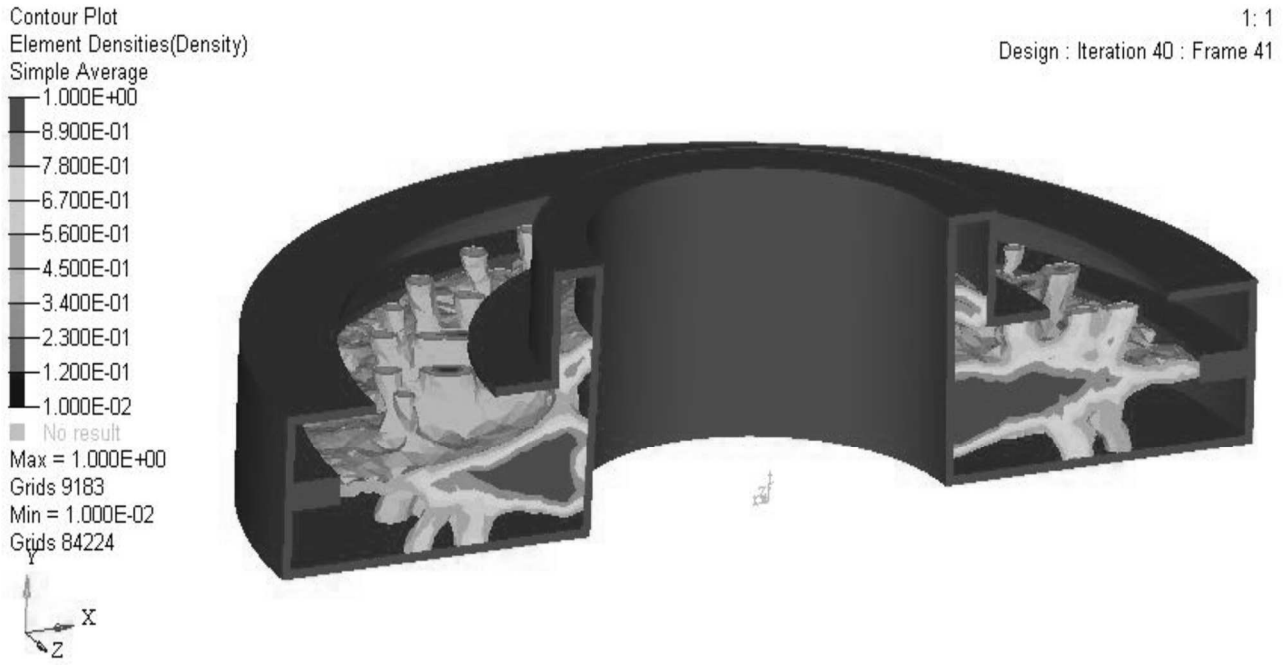

Fig. 9 *Mass distribution obtained for the weighted compliance load case, applying a minimum element size constraint equal to three times the mesh dimension - E*

The impact of modifying the volume fraction used for optimization was therefore tested. In detail, a test run performed with a 15% volume fraction resulted in a distribution of mass that was too fractioned; under these too strict conditions, the integrity of the part was not guaranteed; this solution is not presented in this manuscript as it was deemed not acceptable from the start. A 20% volume fraction value was then considered, introducing also a 200MPa maximum stress limits to be measured on all the elements of the parts in order to assure the structural integrity of the component. This analysis, marked with the letter F, has produced the geometry visible in Fig. 10 and the related results reported in Table 5. As it can be seen from the table, the 200Mpa maximum stress limit was correctly enforced and was arguably felt more heavily to guide the optimal mass distribution for the centrifugal load component.

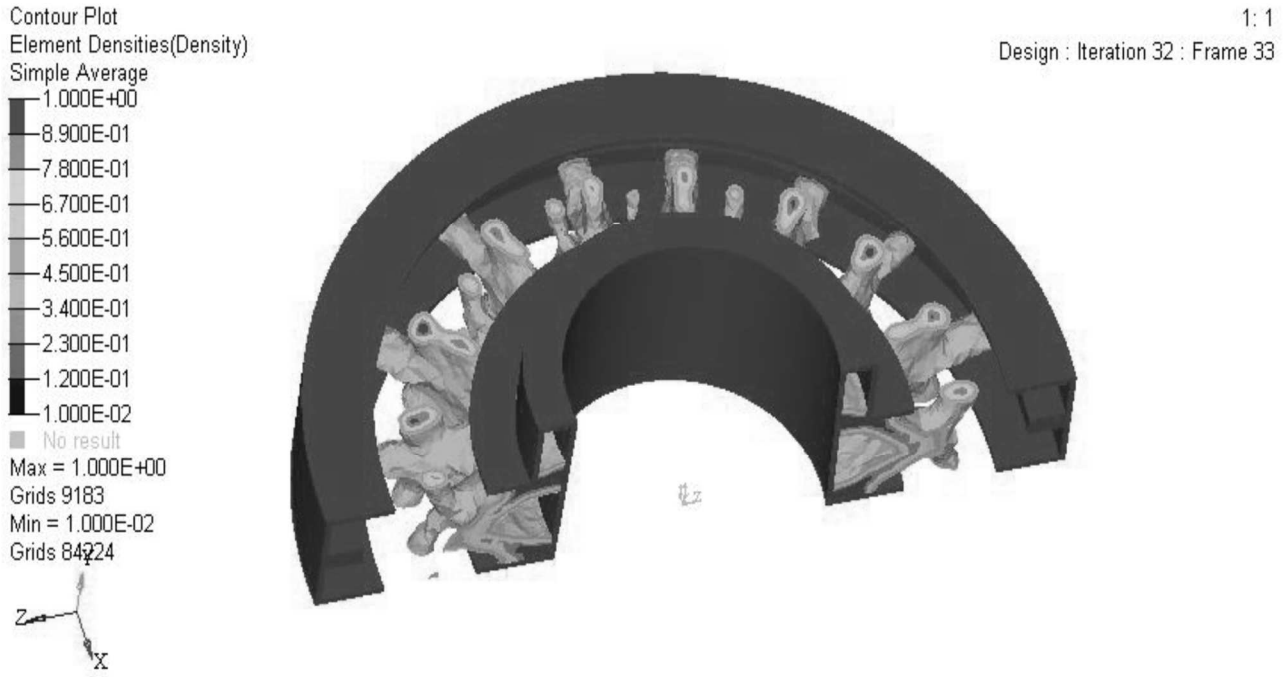

Fig. 10 *Mass distribution obtained for the weighted compliance load case, applying a minimum element size constraint equal to three times the mesh dimension; 20% volume fraction, 200MPa maximum stress – F*

Tab. 5 *Stress and displacements results for the weighted compliance load case, applying a minimum element size constraint equal to three times the mesh dimension; 20% volume fraction, 200MPa maximum stress*

INDEX	Load Case used to drive optimization	Constraint	Response	Verified under		
				Axial Load #1	Axial Load (#2)	Centrifugal Load (#3)
F	Weighted Compliance (1,1,1)	20% volume fraction, min member size = 3*mesh size, max stress 200MPa	Stress (MPa)	149	125	198
			Displacement mag. (mm)	0.0877	0.0871	0.0866

The choice of the final design to be developed depends on multiple factors, such as the manufacturability of the chosen shape. Two conditions were selected to be fully developed and further studied: D and F.

3.3 Non linear optimization

A non linear optimization is required in order to introduce the effects of the interference fit between the shaft and the hub. This is introduced in the analysis by setting a temperature difference between the shaft and the hub. The resulting stress distribution is used as initial condition for the loads that are subsequently applied. At each optimization step the resulting shape will be analyzed once again to compute the updated stresses induced by the force fitting; accordingly, the updated stress distribution will be evaluated in a new non linear analysis.

While the mass distributions obtained in the following tests are similar to the ones previously depicted, a key difference can be observed in the hub region. Linear simulations, which weren't considering coupling forces, tended to remove material from the hub region, which in this case is less emptied.

The nodes on the hub region of the models obtained at the end of the optimization were verified to assure that their displacements are contained in the range imposed by the tolerance (0.0628mm). The imposition of a rigid constraint on the displacement of the hub nodes would have been too heavy to manage for the optimization and would not have brought any additional benefit.

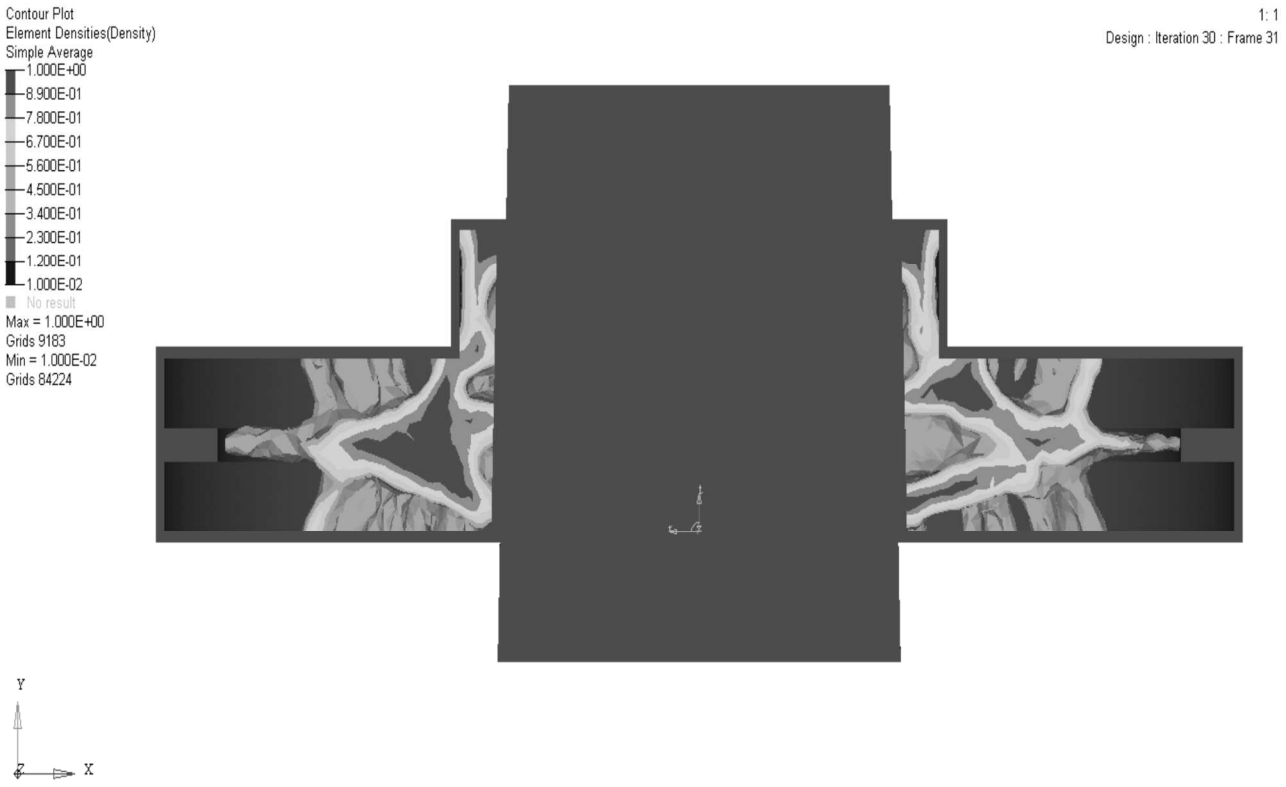

Fig. 11 *Non linear optimization mass distribution for the weighted compliance scenario*

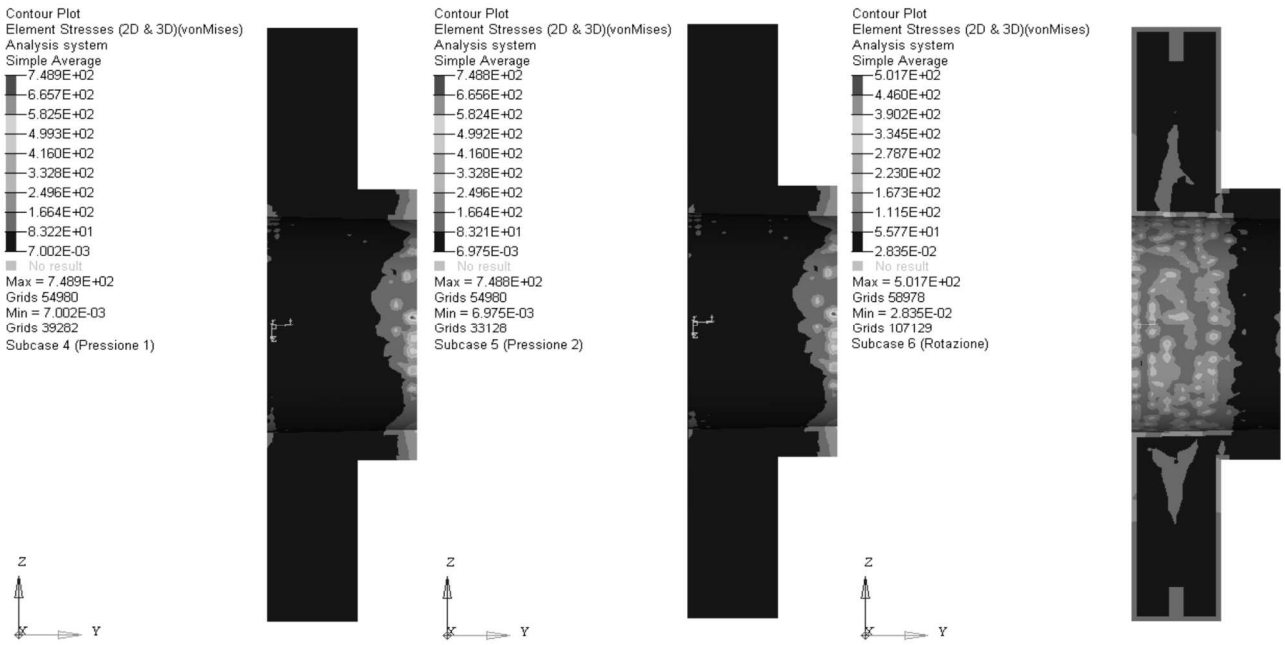

Fig. 12 *Non linear optimization mass distribution for the weighted compliance scenario*

3.4 Lattice optimization

Lattice optimization is carried out in two subsequent steps: in a first step a standard topology optimization is carried out with a reduced density penalty in order to obtain a porous material. A second step starts with the substitution of solid mesh elements with BAR and BEAM elements and the optimization works on the identification of the best truss diameters to assure the imposition of the stress and displacement constraints. A 4 mm mesh size was set to reduce the computational costs of this analysis; furthermore, this change in mesh size allowed to obtain a lattice structure characterized by bigger elements, more suitable for fabrication. The constraint on the maximum stress tolerated during the simulation was modified to assure that the convergence of the analysis: a 400MPa limit was set as maximum stress for the 1D elements, while the same 200MPa constraints was set for solid elements.

Two different scenarios were considered: a hybrid solid/lattice model optimization (analysis #G) and one where the resulting part is composed only by lattice (#H). The two optimizations produced respectively a 59.5% and a 62.5% weight reduction. Fig. 13-20 show the results obtained in the development and FE-analyses of models G and H.

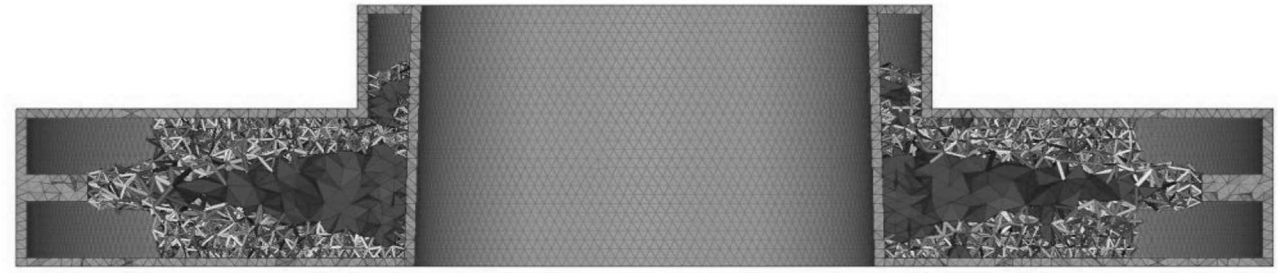

Fig. 13 *Mesh and lattice model obtained in the hybrid solid/lattice optimization G*

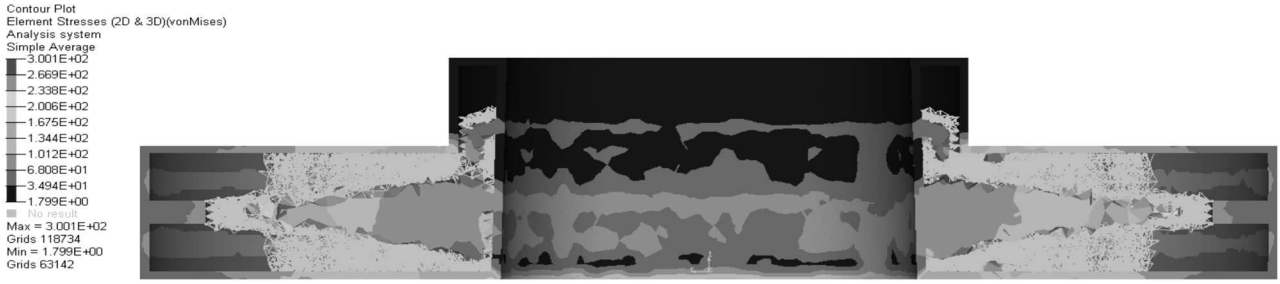

Fig. 14 *Stress values for the solid mesh elements G*

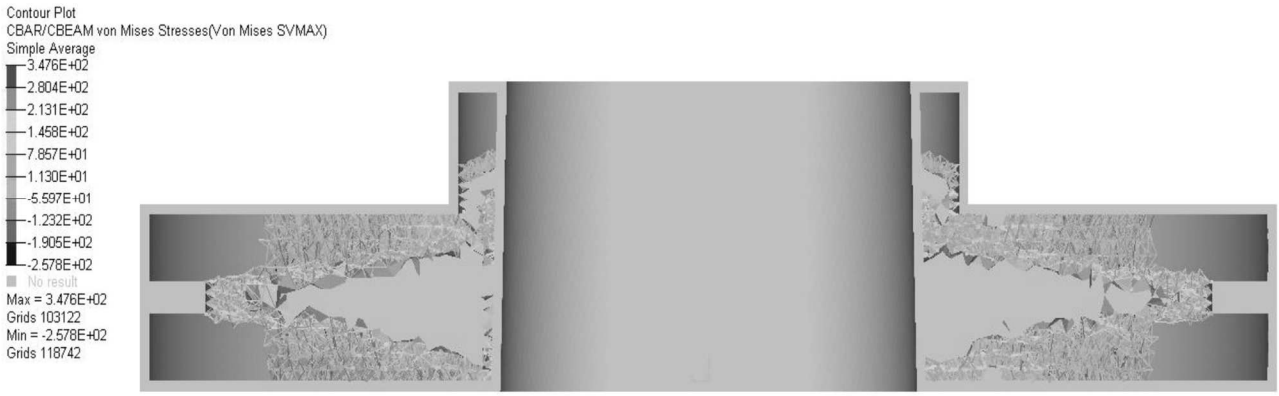

Fig. 15 *Stress values for the 1D elements G*

The displacements obtained on the hybrid model are visible in Fig. 16.

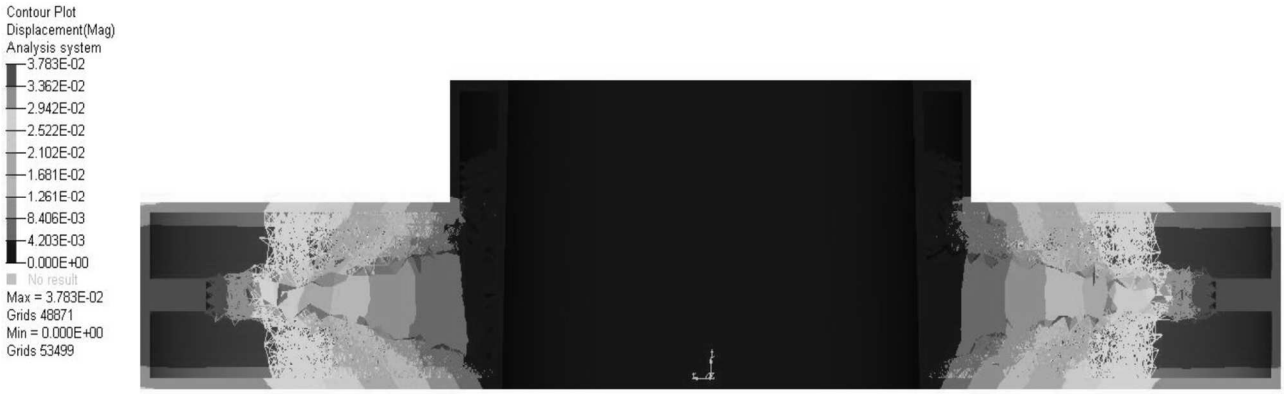

Fig. 16 *Displacements of the hybrid model G*

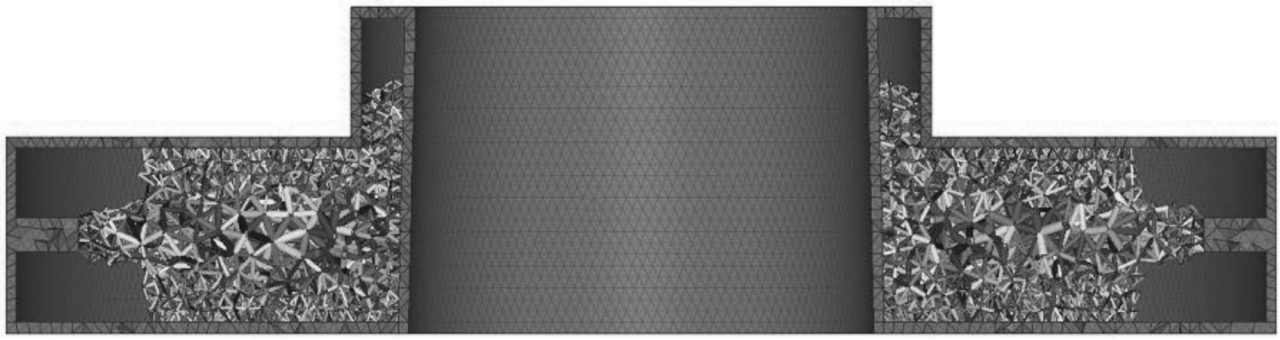

Fig. 17 *Element distribution in the lattice model H*

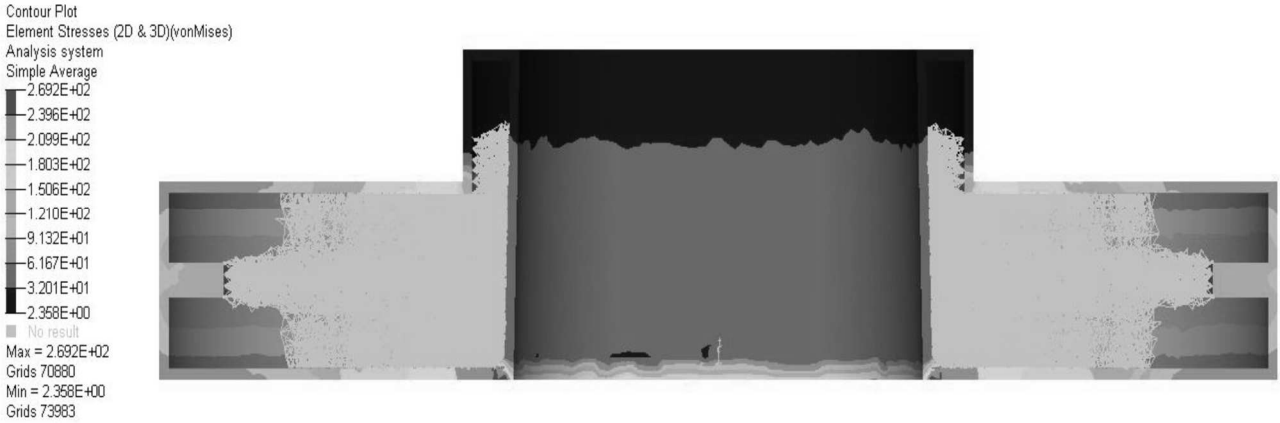

Fig. 18 *Stress distribution for the lattice model, 3D elements H*

Fig. 19 *Stress distribution for the 1D elements of the lattice model H*

Fig. 20 *Displacements of the lattice model H*

4 Dynamic behaviour

Due to its bulky geometry, the thrust collar is not subjected to challenging dynamic conditions. Nevertheless, in order to test the entire procedure that would be useful to optimize the geometry of turbine or compressor rotors, this step was tested even in the present case study.

The disc is modelled as was previously done for the static optimization. The analysis was carried out introducing an harmonic forcing load in the range 0-20000 Hz with magnitude 90000N. 4 nodes positioned on the external rim of the component were selected to read displacements and accelerations; such positions should observe the highest displacements. The optimization imposed a maximum displacement on the nodes of 0.15 mm and was guided by the minimization of the volume (not the weighted compliance, which cannot be used for a purely dynamic case). The stiffness of the component will be verified at the end of the process with a separate analysis. By comparing the two graphs visible in Fig. 21 and Fig. 22 is possible to observe a general reduction of the stiffness of the component and a resulting compaction of resonant frequencies, which are shifted on the left of the graph. The resulting model is depicted in Figure 23.

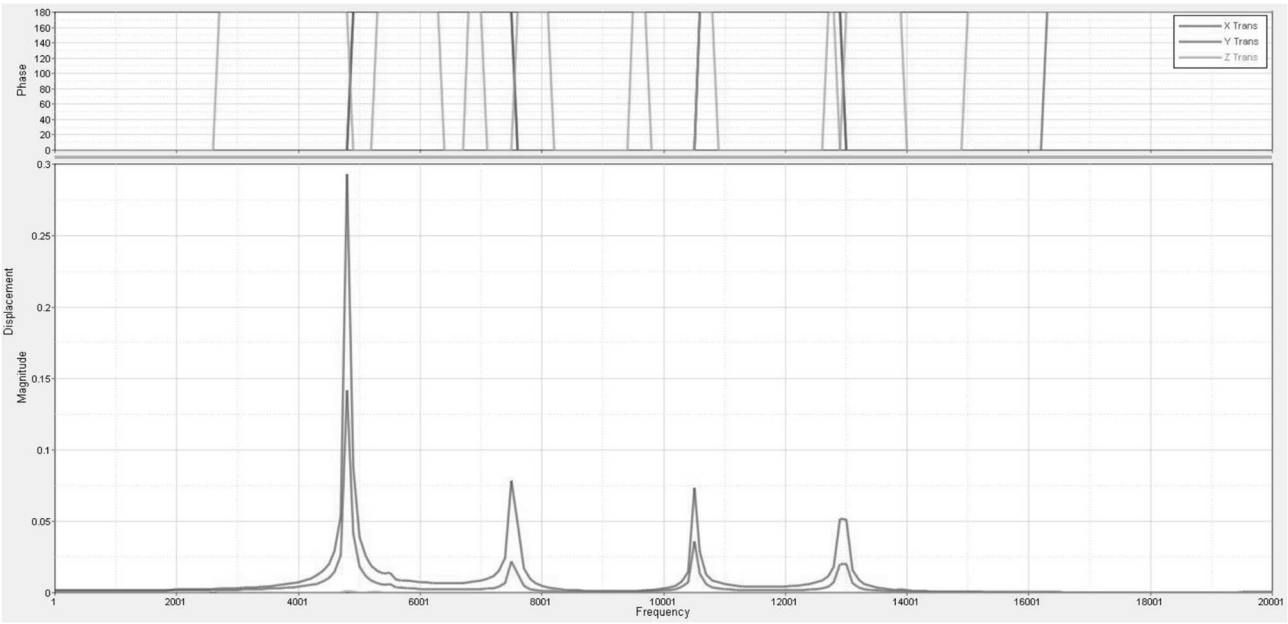

Fig. 21 *Pre-optimization frequency response graph of the node of interest in linear scale*

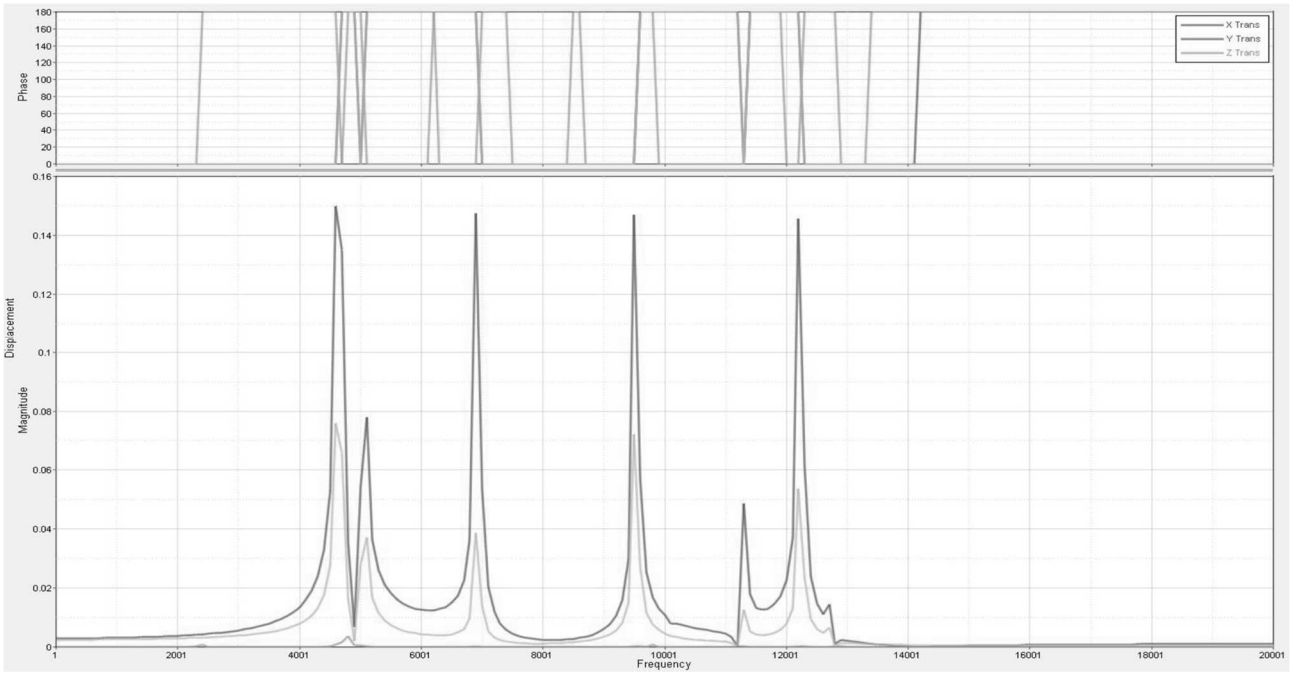

Fig. 22 *Post-optimization frequency response graph of the node of interest in linear scale*

By comparing the two graphs is possible to observe a general reduction of the stiffness of the component and a resulting compaction of resonant frequencies, which are shifted on the left of the graph and more close to each other. The maximum displacement of the considered node is limited to 0.15 mm, as desired. The resulting model is depicted in Fig. 19. This effect is considered beneficial for the application under consideration. With respect to the specific results obtained in this part of the study, it needs to be considered that frequencies in the order of 4000-5000 Hz cannot be easily registered during the work life of this specific component. Accordingly, the integration of the results obtained during the dynamic optimization analysis is not relevant to this specific case.

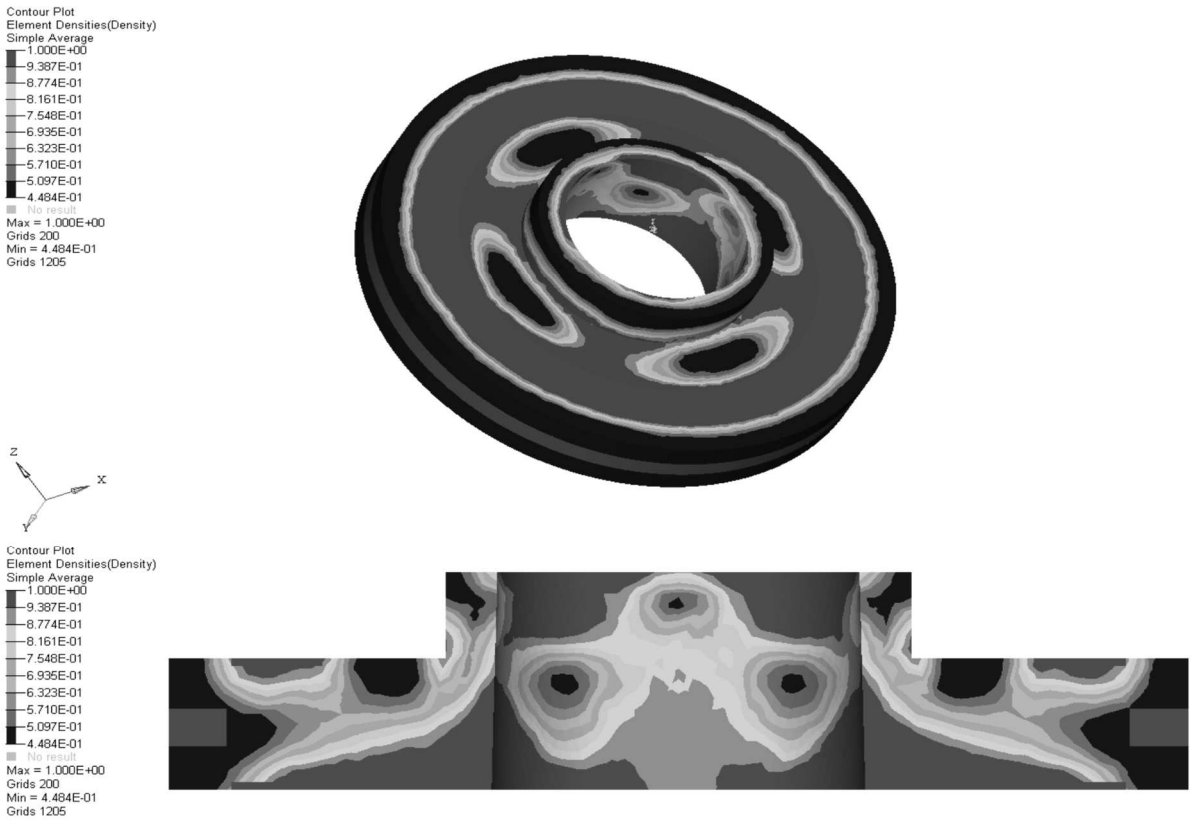

Fig. 23 *Density distribution obtained in the dynamic optimization of the component*

5 Modelling

The models obtained at the end of the FE analyses are not ready to be used for all the subsequent steps; a proper parametric CAD model is required in order to generate a usable and well defined geometry of the component. Accordingly, models D and F were selected as reference and used to drive the modelling of the final versions of the component under examinations. These two analyses were selected as they generated the most interesting solutions.

Hyperview® was used to generate a diametral section of each optimized shape to be used as reference to model the object. The section was imported in Solidworks and used to guide a 2D sketch describing the internal shape of the component. The entire model was reconstructed using revolution functions, imposing axial symmetry and comparing the resulting 3D shape with the mesh model obtained in Hypermesh®. The solid model obtained from the D anlysis is visible in Fig. 24, the solid model derived from the F analysis is depicted in Fig. 25.

Fig. 24 *CAD model of the component "D" (diametral section and 3D rendering of half collar)*

Lattice geometries cannot be processed with the same operations due to the complexity of the shape to be reconstructed. Hypermesh does not allow a direct generation of a 3D lattice model from the FE model. Materialise 3-matic was used to convert the mesh file to a significant model. The transformations generates a mesh model from the FE model used by Hypermesh®. The resulting 3D model, obtained elaborating the Hypermash model obtained using a full-lattice approach, is depicted in Fig 26.

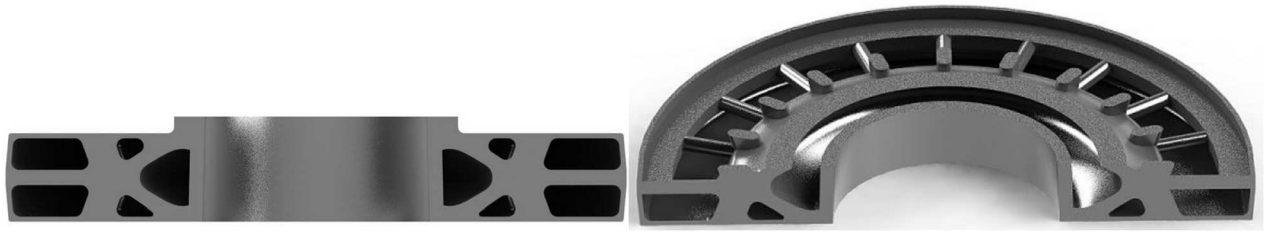

Fig. 25 *CAD model of the component "F" (diametral section and 3D rendering of half collar)*

Fig. 26 *Lattice model diametral section*

This transformation causes the generation of a heavy model, because each truss is converted from a 1D representation into a solid one, where each truss is modelled with a specific diameter identified in the analysis. At the end of the conversion, the mass of the resulting model was compared with the FEM model: no significant differences were identified.

6 Results and conclusions

The three models described in the previous chapter achieved, at the end of the optimization/modeling workflow, significant mass reductions compared with the original component. Fig 27 shows the comparison between the three models on this aspect.

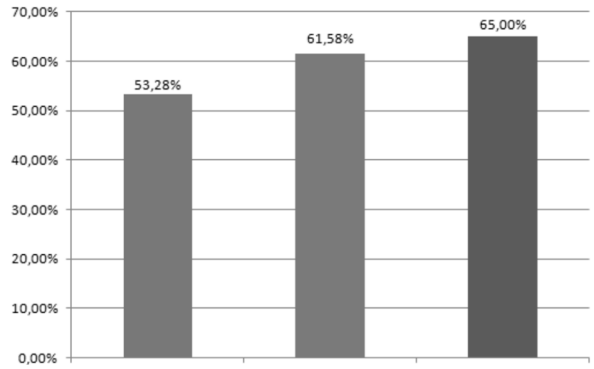

Fig. 27 *Percentage of the reduction of mass achieved by each model: Blue – D; Green – F, Red – Lattice*

The lattice model is the best performing of all three, resulting in a final 65% decrease of the original component weight. The D and H models were selected for a test print to perform a preliminar study on the fabrication problems and characteristics that could affect the development of such peculiar shapes. Figures 28 shows the cross-section of the models built using a Concept Laser M2 Cusing machine; only a quarter of the original models were printed in order to save time and material. The test highlighted some problems regarding the deformations introduced by the residual stresses accumulated during the AM process, which are visible even at the naked eye and need to be improved to allow the fabrication of the real components. While the print of a quarter of the entire model could have affected the quality of the produced test model by introducing different deformations in the process, this effect need to be considered and mitigated. The effect is most visible on the H model, but smaller errors are present even in the other configurations.

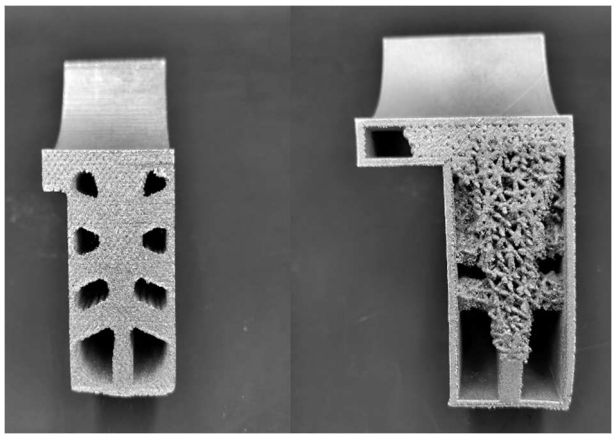

Fig. 28 *Cross section fabricated for models D and H*

A first intervention, with this respect, might be the introduction of fillets on all internal corners to improve the regularity of the model and smooth the transitions between areas characterized by different densities and, hence, higher residual stresses. Subsequently, the introduction of a thicker shell for the part should have a beneficial effect on deformations. A more refined and time consuming strategy could exploit a topology optimization analysis that takes into account even a manufacturability optimization, such as a reduction of the internal stresses that arise during fabrication. Interesting approaches that have been presented at the state of the art on this topic are described in [7], [8].

Additional aspects that will be tackled in a future detailed design phase will be the implementation of design features that can allow the removal of unsintered powders in the printed part, as full parts will not allow access to the internal empty volumes for powder removal. Computer-based tools to support the designer in determining the bast strategy to account for powder removal were developed to avoid time consuming trial and error approaches [9]. Considering manufacturing needs, postprocessing will require a detailed design phase tackling the optimization of thermal processes as proposed in [10].

References

[1] L. DENTI, A. SOLA, S. DEFANTI, C. SCIANCALEPORE, AND F. BONDIOLI, "Effect of powder recycling in laser-based powder bed fusion of Ti-6Al-4V," *Manufacturing Technology*, vol. 19, no. 2, pp. 190–196, 2019, doi: 10.21062/UJEP/268.2019/A/1213-2489/MT/19/2/190

[2] T. MACONACHIE et al., "SLM lattice structures: Properties, performance, applications and challenges," *Mater. Des.*, vol. 183, p. 108137, Dec. 2019, doi: 10.1016/J.MATDES.2019.108137

[3] G. FAYAZ AND S. KAZEMZADEH, "Towards additive manufacturing of compressor impellers: 3D modeling of multilayer laser solid freeform fabrication of nickel alloy 625 powder mixed with nano-CeO2 on AISI 4140," *Addit. Manuf.*, vol. 20, pp. 182–188, Mar. 2018, doi: 10.1016/J.ADDMA.2018.02.001

[4] E. MELI, R. FURFERI, A. RIND, A. RIDOLFI, Y. VOLPE, AND F. BUONAMICI, "A General Framework for Designing 3D Impellers Using Topology Optimization and Additive Manufacturing," *IEEE Access*, vol. 8, pp. 60259–60269, 2020, doi: 10.1109/ACCESS.2020.2982841

[5] E. MELI et al., "Design and production of innovative turbomachinery components via topology optimization and additive manufacturing," *Int. J. Rotating Mach.*, vol. 2019, 2019, doi: 10.1155/2019/9546831

[6] A. W. GEBISA AND H. G. LEMU, "Additive Manufacturing for the Manufacture of Gas Turbine Engine Components: Literature Review and Future Perspectives," in *Volume 6: Ceramics; Controls, Diagnostics, and Instrumentation; Education; Manufacturing Materials and Metallurgy*, Jun. 2018, p. V006T24A021, doi: 10.1115/GT2018-76686

[7] G. ALLAIRE AND L. JAKABAIN, "Taking into account thermal residual stresses in topology optimization of structures built by additive manufacturing," *https://doi.org/10.1142/S0218202518500501*, vol. 28, no. 12, pp. 2313–2366, Nov. 2018, doi: 10.1142/S0218202518500501

[8] S. XU, J. LIU, AND Y. MA, "Residual stress constrained self-support topology optimization for metal additive manufacturing," *Comput. Methods Appl. Mech. Eng.*, vol. 389, p. 114380, Feb. 2022, doi: 10.1016/J.CMA.2021.114380

[9] A. ROBERTS, R. KAHRAMAN, D. BACHEVA, AND G. TABOR, "Modelling of Powder Removal for Additive Manufacture Postprocessing," *J. Manuf. Mater. Process. 2021, Vol. 5, Page 86*, vol. 5, no. 3, p. 86, Aug. 2021, doi: 10.3390/JMMP5030086

[10] H. JIRKOVÁ, K. OPATOVÁ, L. KUČEROVÁ, I. ZETKOVÁ, Š. JENÍČEK, AND K. BURDOVÁ, "Effects of Heat Treatment on Microstructural Evolution in Additively-manufactured Parts of Various Heights from Maraging Steel," *Manufacturing Technology*, vol. 22, no. 1, pp. 14–19, 2022, doi: 10.21062/MFT.2022.008